Article ID: 1006-8775(2019) 01-0001-10

# A MODELING STUDY OF INHOMOGENEOUS COASTAL GALES ASSOCIATED WITH THE LANDFALL OF TYPHOON SOUDELOR (2015)

ZHU Ye (朱 业)[1, 2], ZHANG Hong-lei (张红蕾)[2], CHEN You-li (陈有利)[3],
ZHAI Guo-qing (翟国庆)[2], LIU Rui (刘 瑞)[2]
(1. Zhejiang Center for Ocean Monitoring and Prediction, Hangzhou 310007 China;
2. Department of Atmospheric Sciences, School of Earth Sciences, Zhejiang University, Hangzhou 310027 China;
3. Ningbo Weather Bureau, Ningbo 315000 China)

**Abstract:** In this study, coastal gales and rainfall attributed to the landfall of Typhoon Soudelor (2015) are analyzed based on observational dense automatic weather stations data, advanced scatterometer-retrieved 10-m ocean surface wind data and simulations using the Weather Research and Forecast (WRF) model. This study focuses on gale bands in the right-front quadrant of the typhoon and associated coastal winds over Zhejiang and Fujian Provinces in China before the landfall of the typhoon. The results are summarized as follows. (1) 10-m surface wind data from automatic weather stations over land and islands, advanced scatterometer-retrieved 10-m ocean surface wind data, and the WRF simulation indicate similar mesoscale offshore gales. (2) The model simulation with a 333-m grid mesh indicates a gale zone over the right-front quadrant of the typhoon; the gale is "broken" over the coastal areas, and formed an inhomogeneous gale band. (3) The model-simulated winds agree well with the island observations. (4) Non-uniform gales over boundary layers result in horizontal wind-speed gradients and strong convergence that favors the development of convection and the maintenance of ocean surface gales.

**Key words:** ocean surface gale; Typhoon Soudelor; severe convection; WRF model; Inhomogeneous field
**CLC number:** P444 **Document code:** A
doi: 10.16555/j.1006-8775.2019.01.001

## 1 INTRODUCTION

China has over 30,000 km of coastline. Coastal areas are often affected by gales associated with weather systems such as typhoons, cyclones moving to the sea, fronts, and severe storms (Xin[1]; Yan et al. [2]). The physical processes responsible for forming offshore gales are complex and involve geologic location, surface conditions, climatic and weather systems. Thus, the formation and prediction of offshore gales is an important research topic in the atmospheric and oceanic sciences. The formation of gales may be associated with increased pressure gradient and the development of low pressure systems(Streten[3-4]; Loewe[5]). Reid studied the relationship between cold southerly winds off the shore of southeastern Australia and surface temperature over coastal terrain[6]. Mass et al. found that the special topography of the strait leads to the formation of large pressure gradients, which result in gales at the strait's exit and downstream[7]. Miglietta et al. analyzed gales over the Mediterranean Sea and showed that islands generate gravity waves, which affect offshore gales and weather[8]. Sheng et al. used numerical modeling to study gales over China's Bohai Sea and revealed that the topography of northern Bohai Sea enhances northeasterly gales[9].

During summer, typhoons are major weather systems causing offshore gale in the Northern Hemisphere and disasters over coastal areas (Chen and Ding [10]). Yang and Lei conducted a statistical analysis of China offshore gales by using 50-year data and found that typhoon-induced gales mainly occur in the southern part of the Bay of Hangzhou in Zhejiang Province[11]. The gales are not uniformly distributed and mainly appear in the eastern quadrant of typhoons before landfall (Lee and Marks[12]; Chen et al.[13]), which may be related to the asymmetric distributions of the physical quantities associated with typhoons (Liu et al.[14]; Zhao et al.[15]). Based on wind data from two meteorological towers and one mobile wind profile at Qiongzhou Strait, Wang et al. analyzed the gales associated with Typhoon Neadat (2011) and found that the gales in the right-front quadrant of the typhoon were gusty[16]. Zhu et al. conducted a sensitivity experiment and found that the horizontal surface wind speed has a well-organized distribution with pairs of streamwise maximum and minimum wind bands aligned at a slight angle to the wind direction [17]; these findings are similar to the radar-observed roll vortices reported by Morrison et al.[18] since mesoscale gales and speed differences are important factors in the formation of roll vortices.

**Received** 2017-11-25; **Revised** 2018-12-04; **Accepted** 2019-02-15
**Foundation item:** National Natural Science Foundation of China (41575042)
**Biography:** ZHU Ye, M.S., primarily undertaking research on tropical cyclones.
**Corresponding author:** LIU Rui, e-mail: liurui_geo@zju.edu.cn

The East China Sea is a busy trade zone and hosts important oversea trade harbors for Zhejiang and Fujian Provinces. It is often affected by offshore gales, particularly those caused by typhoons. Recently, numerical models have been used to predict offshore gales over the sea (Ji et al.[19]; Gilliam et al.[20]; Miglietta et al.[21]; Chen et al.[22]). Although many studies have been conducted on offshore gales, few studies have examined the mesoscale features of offshore gales. In this study, we simulate Typhoon Soudelor (2015), which damaged the coastal areas of Zhejiang and Fujian Provinces, to analyze the evolution of mesoscale speed associated with the typhoon. An overview of Typhoon Soudelor is given in Section 2. The setup of the numerical experiment is discussed in Section 3, and the results are presented in Section 4. Section 5 presents the conclusions.

## 2 OVERVIEW OF TYPHOON SOUDELOR AND EXPERIMENT SETUP

### 2.1 *Overview of typhoon Soudelor*

Typhoon Soudelor formed over the northwestern Pacific at 12:00 UTC on July 30, 2015 and moved westward. It was upgraded to a super typhoon with a minimum pressure of 910 hPa and a maximum wind speed (MWS) of 65 m $s^{-1}$ at 02:00 UTC on August 3, 2015. When it landed at Xiulin, Hualian, Taiwan on August 7, 2015 at approximately 16:40 UTC, the minimum pressure was 940 hPa and the MWS was 48 m $s^{-1}$. It passed over the Taiwan Strait and landed at Xiuyu, Putian, Fujian on August 8, 2015 at approximately 10:10 UTC with a minimum pressure of 970 hPa and a MWS of 38 m $s^{-1}$. After the landfall, Typhoon Soudelor gradually weakened to a tropical depression over Jiangxi Province at 11:00 UTC on August 9, 2015, and to a low pressure center over Anhui Province at 05:00 UTC on August 10, 2015. During landfall, gusty winds of 34 m $s^{-1}$ occurred over the coastal areas of Zhejiang and Fujian Provinces, severely damaging thousands of houses. In Zhejiang and Fujian Provinces, approximately 4.87 million people were affected by the typhoon, leaving 21 dead and 7 missing. The direct economic loss was 15 billion *yuan* (RMB).

### 2.2 *Numerical experiment setup*

The Weather Research and Forecast (WRFv3.7.1) model was used to study the development of mesoscale gales and convective clouds over coastal areas during the landfall of Typhoon Soudelor. The FNL data of the National Centers for Environmental Prediction (horizontal grid = 1° × 1°; time interval = 6 h, accessed at https://rda.ucar.edu/datasets/ds083.2/#!access) were used in this study. Five nested domains (d01, d02, d03, d04, and d05; Fig.1) were designed with horizontal grids of 27 km, 9 km, 3 km, 1 km, and 333 m, respectively, and corresponding horizontal grid points of 191 × 201, 274 × 238, 304 × 313, 460 × 469, and 748 × 825. In this study, we set two experiments with 35 and 57 vertical levels, respectively. The features of the simulated system when using 57 vertical levels is generally similar to that at 35 vertical levels. Because of the similarity, the following analy-

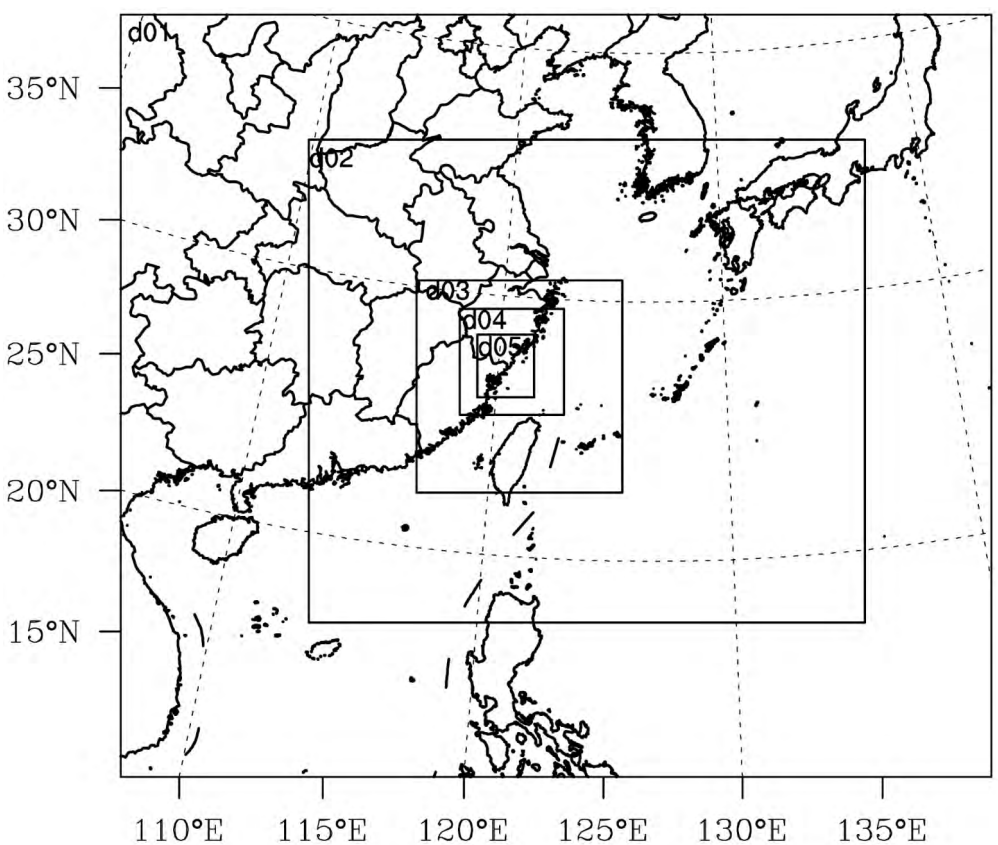


**Figure 1**. Map of model domains d01-d05.

sis is mainly based on the experiment with 35 vertical levels, except the Fig 3c. The time step of 60 s in d01 with the time step ratio of 1:3:3:3:3 for the nested domain was integrated from 12:00 UTC on August 7, 2015 to 12:00 UTC on August 9, 2015 (a total of 48 h) with outputs every 1 h for d01 and d02 and every 10 min for d03, d04, and d05. The model included parameterization schemes for Lin microphysics scheme (Lin et al.[23]), the Dudhia shortwave radiation scheme (Dudhia[24]), Rapid Radiative Transfer Model (RRTM) longwave radiation shceme (Mlawer et al.[25]), five-layer thermal diffusion land surface (Dudhia[26]), and Kain-Fritsch cumulus scheme in domain 1 and 2 (Kain[27]).

## 3 RESULTS

### 3.1 *Typhoon track and rainfall amount*

Figure 2a shows the track of Typhoon Soudelor based on observation and simulation. The observational best track data comes from the Shanghai Typhoon Institute. The simulated track generally agrees with the observed track, except for the southwestward movement in the simulation track when Typhoon Soudelor passes over Taiwan. We use the average absolute deviation and the root mean square error (RMSE, Carvalho et al.[28]) to quantify the differences. For the typhoon track forecast skill, the average absolute deviation is 0.40°, and the RMSE is 0.19. The average absolute deviation of the MSLP is 6.3 hPa, and the RMSE is 5.8.

Rainfall mainly occurred over the coastal areas of southern Zhejiang and northern Fujian during the landfall of Typhoon Soudelor. The observational data comes from dense automatic weather stations, which is provided by the China Meteorological Administration. The observation shows that heavy rainfall (300 mm/day) mainly appeared along the coastline from 00:00 UTC on August 8, 2015 to 00:00 UTC on August 9, 2015 (Fig.2b). The simulated rainfall (Fig.2c) was similar to the observed rainfall, although the model slightly overestimated the rainfall amount.

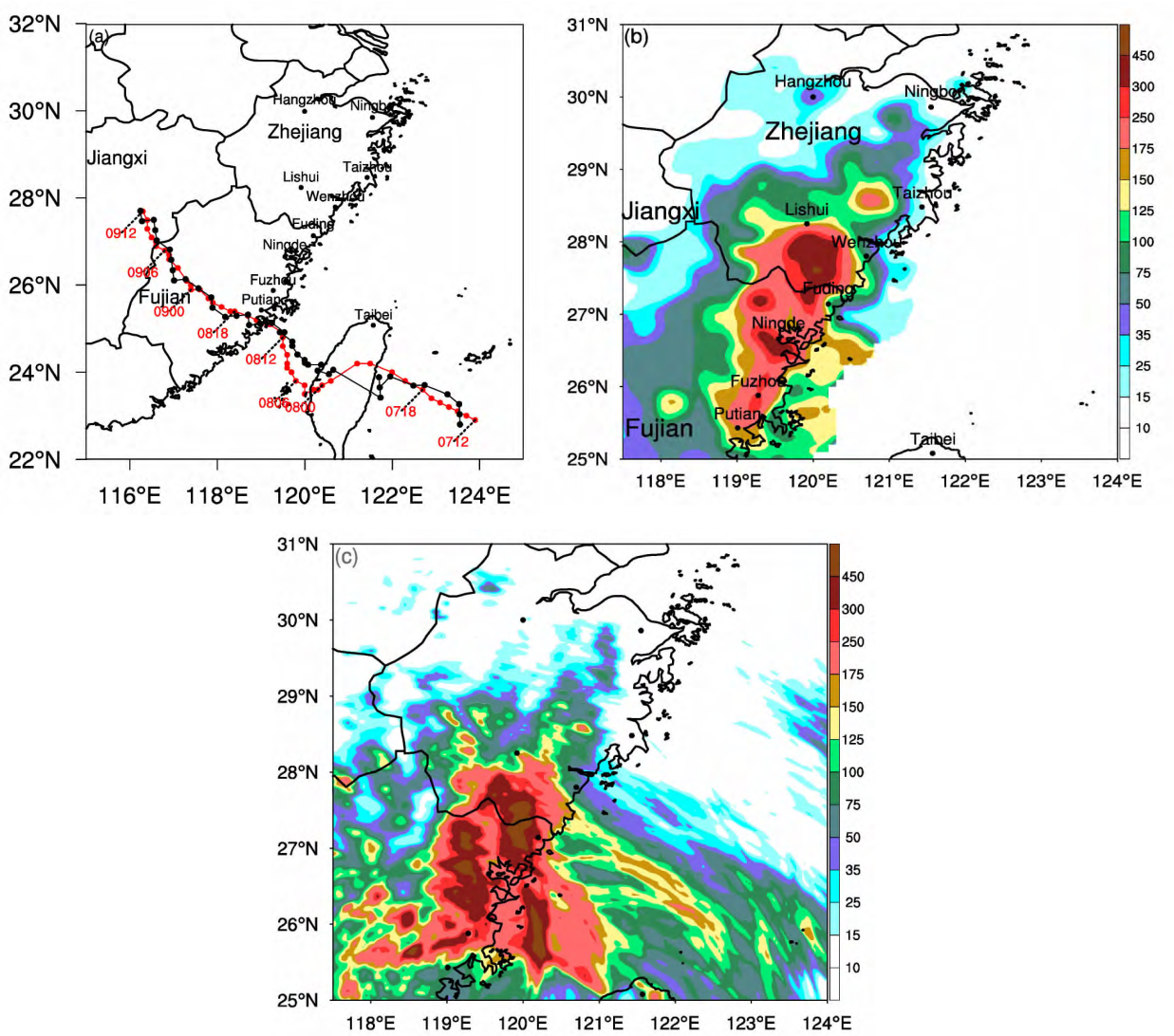


**Figure 2.** (a) Simulated (black) and observed (red) tracks of Typhoon Soudelor and 24-h (from 00:00 UTC August 8, 2015, to 00:00 UTC August 9, 2015) cumulative rainfall amounts from (b) observational data and (c) simulation results in domain d05.

3.2 *Mesoscale gales offshore of Zhejiang and Fujian Provinces*

Since no observational data are available over the ocean, the 10-m ocean surface wind data retrieved from the Advanced Scatterometer(ASCAT) of the European Space Agency (accessed at www.remss.com/missions/ascat) was used in this study. Zhang et al.[29] conducted a validation study and found that the ASCAT wind data over China's offshore areas are reliable. Both the ASCAT data (Fig.3a) and the observational data over land were interpolated into 3-km grids and merged into one observational data set (Fig.3b).

The ASCAT wind data show that when Typhoon Soudelor approached Xiuyu, Putian, Fujian at 09:30 UTC on August 8, 2015, two gale bands were located to the north of the typhoon (bold black arrows in Fig.3). The observational wind data over the land and islands reveal that gale zones with wind speeds exceeding 20 m $s^{-1}$ mainly occurred offshore of Putian and Ningde, Fujian. Similar gale bands can also be found in the retrieved data, in which gale wind speed exceeded 25 m $s^{-1}$, and the horizontal range of massive high-wind-speed center is approximately 50—100 km. Fig.4a shows a strong easterly wind band offshore of Ningde. A weak easterly wind band originating in Taipei, Taiwan can be validated by the observational data. The wind speed offshore of Fuzhou was generally lower than 15 m $s^{-1}$, which is consistent with the ASCAT data. This indicates weak wind bands between the two strong wind bands in Ningde and Putian, Fujian. Fig. 4b clearly suggests offshore locations of the gale-band centers, Typhoon Soudelor-induced mesoscale wind-speed centers, weak wind bands and non-uniform mesoscale gales over the bays offshore, and a rapid decrease in offshore gales. Fig. 4c showed the simulated wind field in d03 at 09:30 UTC on August 8, 2015. The simulated results were similar to the observational data (Fig.3b); the simulation produced similar locations of the two gale bands (bold black arrows), weak wind bands between the two gale bands, and a rapid decrease in the strength of the offshore gales strength (Fig. 3c).

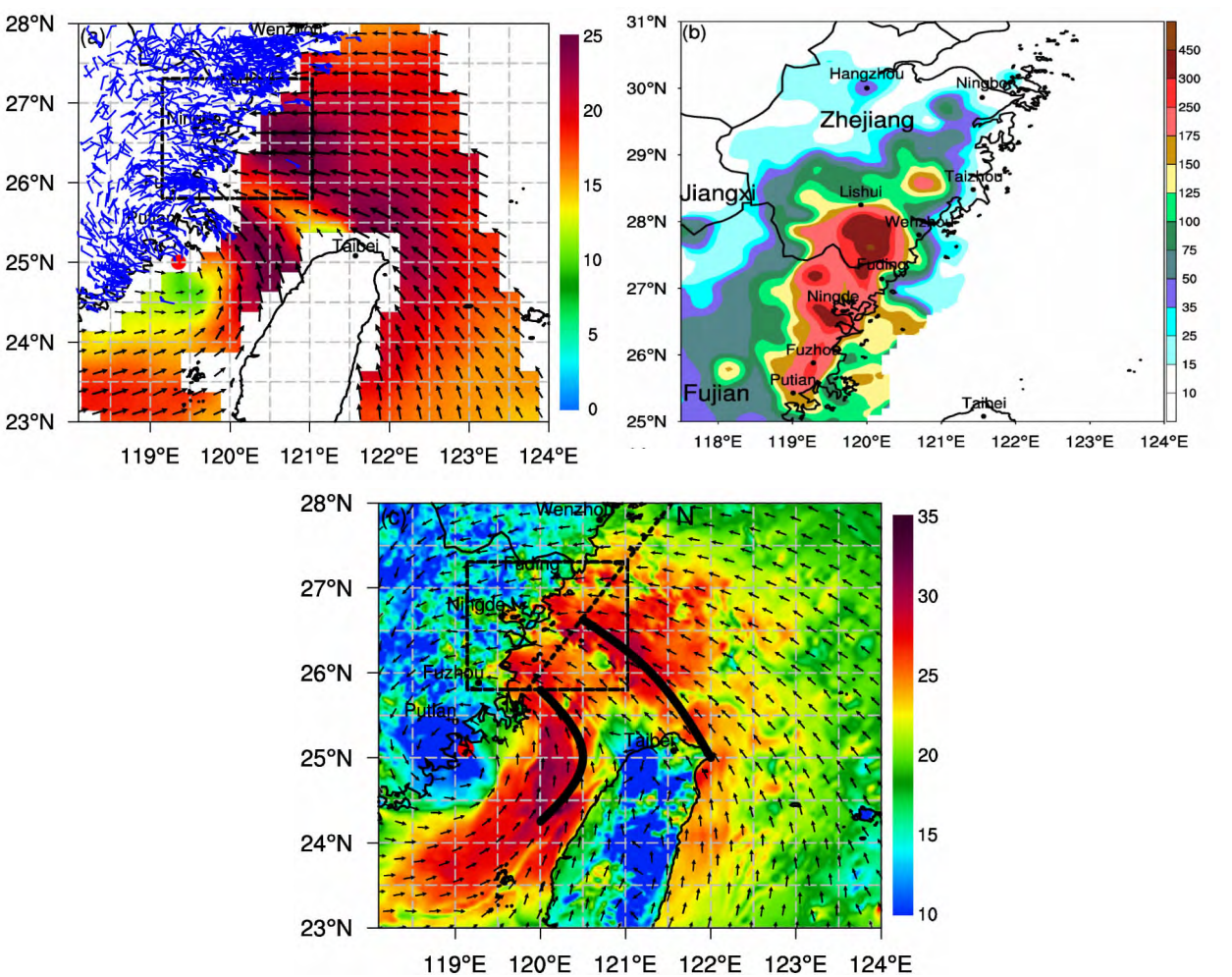


**Figure 3**. Horizontal wind distributions when Typhoon Soudelor approached Putian, Fujian, based on (a) ASCAT-retrieved wind data over the ocean and from auto-weather stations over land, (b) observation data interpolated into a 3 km grid, and (c) simulations in domain d03 at 09:30 UTC August 8. The box covers the coastal areas of northern Fujian and southern Zhejiang. The colored background denotes wind speed (m $s^{-1}$). The red typhoon marker denotes the center of Typhoon Soudelor. The bold black line shows the maximum coastal wind. M-N in (c) is used to plot the cross section in Fig.7.

To conduct an in-depth analysis of the mesoscale structures of offshore gales, the gales in the right-front quadrant of the offshore areas of northern Fujian and southern Zhejiang (dashed boxes in Fig.3) just before the landfall of Typhoon Soudelor were plotted (Fig.4). The observation data are the 10 m ocean surface wind data retrieved from the ASCAT with 25 km horizontal resolution which is shown for the sea, and the wind data from the surface meteorological station in the Chinese mesonet which is plotted for land. Both the observational data and simulation results in d05 revealed offshore gales with wind speeds of over 20 m $s^{-1}$ (see ①–⑤ in Fig.4). Compared to the observational data, the simulation predicted a weaker gale in Changchun (②). Over the bay near Sandu (④), the model indicated that a gale passed over the offshore area to the bay. Tantou(⑤) located a gale band near the center of Typhoon Soudelor (Fig.4a). ⑥, ⑦, and ⑧ display weak winds. The simulation in d05 also indicated a decrease in wind speed over these regions (Fig.4b), suggesting that islands, complex coastal terrain, and the intensity of convection contribute to the non-uniform horizontal distribution of gales. The wind pattern exhibits mesoscale structures, which shows the characteristics of nonuniform gusty winds. The phenomenon of gusty winds lasted for a certain period. Fig. 5b shows the horizontal scale of 10-30 km.

The simulated wind field also displays mesoscale structures along the complex coastline. The horizontal scale of a gale become large when the gale moves to a bay area such as Sandu, Ningde, Fujian(④), whereas it decreases when the gale moves to a mountainous area, resulting in a non-uniform distribution. Such a distribution is well represented in both the observational and simulated data. Thus, the gusty and massive offshore gales seem to be broken, which may show the existence of mesoscale pulse signal of wind speed. In the following section, we will use observational data and simulation results to check whether the mesoscale pulse signal of wind speed exists.

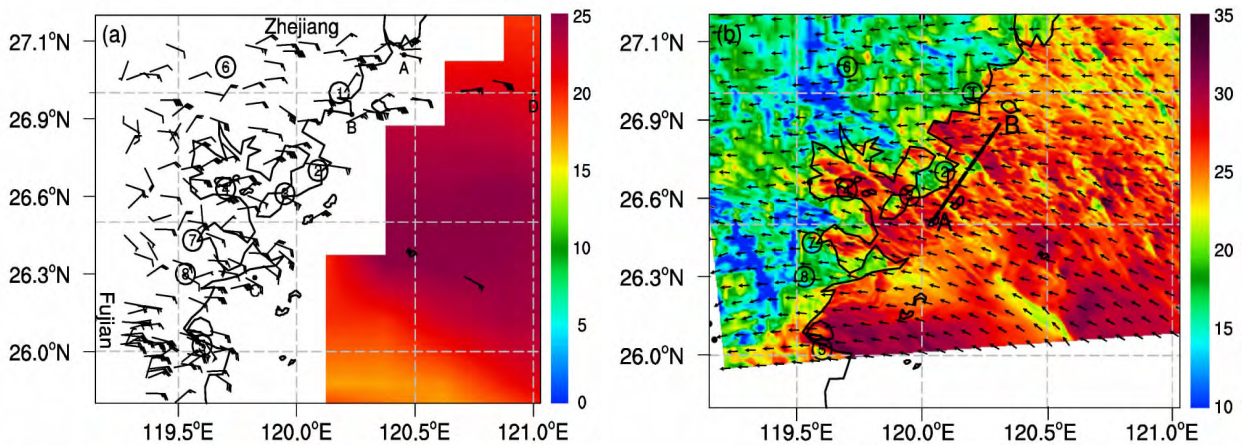


**Figure 4**. Horizontal distributions of winds based on (a) observational data and (b) simulation in domain d05. In (a), A, B, C, and D denote the positions of the four islands in Figs. 5 and 6. ①–⑧ denote the positions of coastal towns in Ningde, Fujian; ①–⑤ show Shansha, Changchun, Xiahu, Sandu, and Tantou, respectively, and ⑥–⑧ denote zones of weak wind. A-B in (b) was used to plot the cross-section in Fig.8.

## 4 COMPARISON OF WIND FIELD AT COASTAL AND ISLAND STATIONS

The wind fields (Fig.5) at four island stations near the gale bands were compared (A, B, C, and D in Fig.4a). The simulation results generally follow the observational data for the four stations and suggest that Typhoon Soudelor moved northwestward and made landfall, after which the winds switched from northeasterly to southerly. When the wind direction turned clockwise, the observational data show few fluctuations with small amplitudes. In contrast, the simulated wind directions do not show any fluctuation, although both observation and simulation suggest a similar evolution in wind direction.

Compared to the change in wind direction, the temporal change in surface winds is more complex (Fig. 6). Both observation and simulation show increases and decreases in wind speed during the 48-h study period (from 12:00 UTC August 7, 2015 to 12:00 UTC August 9, 2015), although the simulated wind speeds are larger than the observed wind speeds. The wind speeds observed at stations have long-lasting increases and decreases along with large horizontal areas, and the wind speeds themselves show short-term pulses. The four islands have different locations relative to Typhoon Soudelor and the associated gale zones. Stations B and C are located to the south and north of the gale bands. The observed wind speeds increased at 14:00 and 09:00 UTC on August 8, 2015 and reached the maximum speed of 30 m $s^{-1}$. Since station A was located away from the gale bands, the wind speed increased relatively slowly (Fig.6a) at this station, as shown by the observational data. The wind speed of station A reached 24 m $s^{-1}$. At station D, a MWS of 23 m $s^{-1}$ was observed at 10:00 UTC on August 8, 2015 (Fig. 6d). This indicates that the ocean surface winds near the gale zones increase rapidly and the horizontal gradients of wind speeds are large. Station A, which was 50 km away from the gale zone, showed low wind speeds and a

moderate increase. The simulated evolution of wind speed is similar to the observational data (e.g., Figs. 6b and 6c), although some differences in phase are observed (e.g., Figs. 6a and 6d).

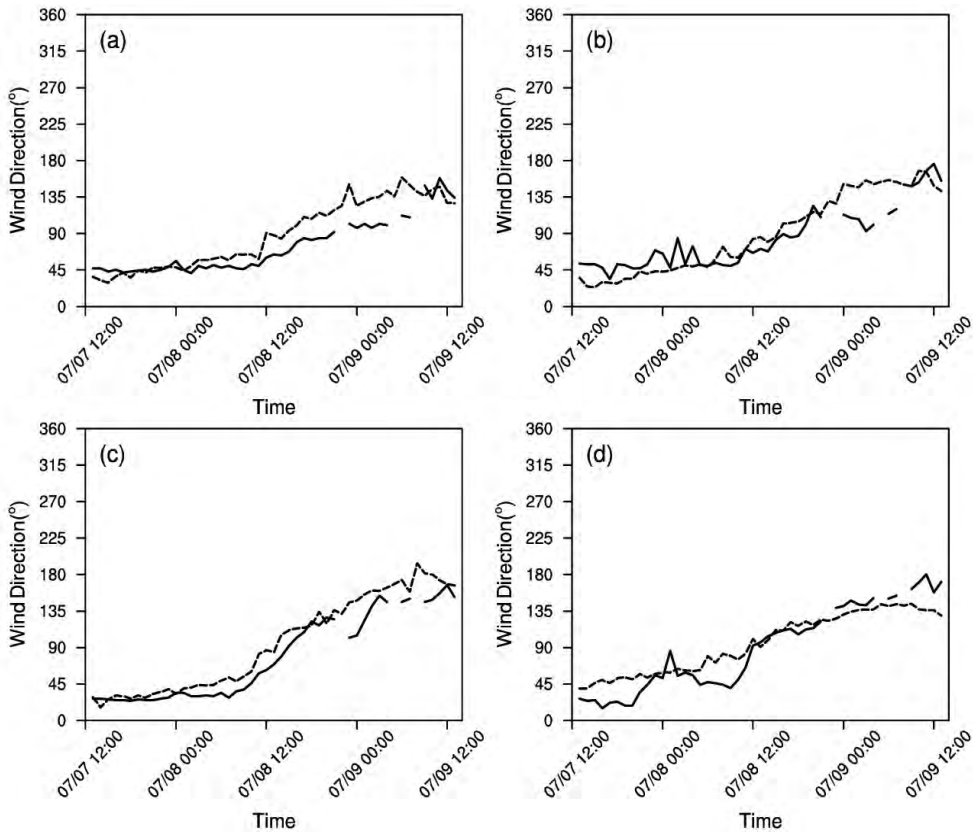


**Figure 5**. Time series of 10 min-averaged wind directions based on observational data from stations on the islands in Fig. 5 (solid line) and simulation in domain d05 (dashed line). The abscissa shows the time period from 12:00 UTC on August 7, 2015 to 12:00 UTC on August 9, 2015, with 10 min intervals. The ordinate shows wind direction (degree).

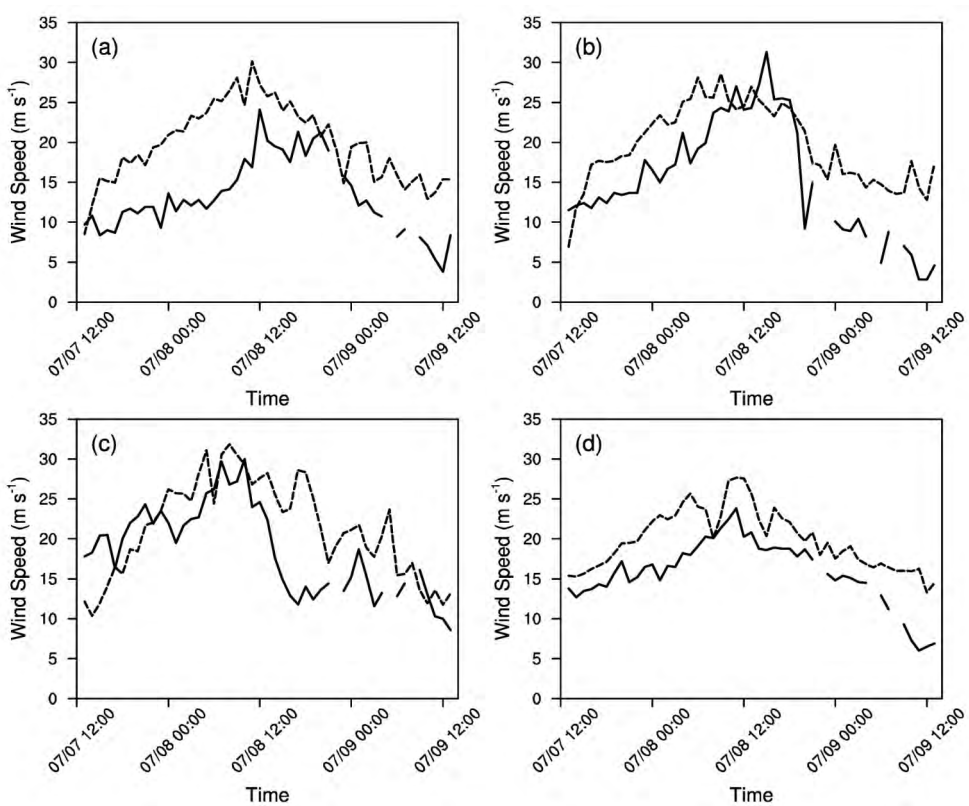


**Figure 6**. Same as Fig. 5 except for wind speed (m $s^{-1}$).

Another mesoscale characteristic of the gale bands is short-term pulses in wind speed during the change in ocean surface winds. The magnitudes of these pulses were approximately 5 m $s^{-1}$. The pulses were random and did not show any periods of oscillation. The pulses were found in both the simulated and observational data and are consistent with those observed during the landfall of Typhoon Neasat[16]. Pulses were also observed in strong westerly winds events in the Strait of Juan de Fuca of Washington State[7]. This may indicate the presence of mesoscale gales over typhoon gale zones because the pulses at stations are not in phase. Thus, Figs. 7 and 8 may demonstrate non-uniform gale massive texture in the simulation with fine-grid mesh.

## 5 STRUCTURES OF OFFSHORE GALES

We used the simulated wind data for d03 at 09:40 UTC on August 8, 2015 to plot a cross-section along M-N in Fig.3c. Fig.5 indicates that the gales were mainly distributed in the northern quadrant over coastal areas. Two gale zones with wind speeds over 40 m $s^{-1}$ were observed south of 26.3°N (coastal areas near Fuzhou) and in the range of 26.3°N–27°N (coastal areas near Ningde). The Fuzhou gale zone was found in the planetary boundary layer and lower troposphere, whereas the Ningde gale zone was mainly observed in the planetary boundary layer. The M–N cross-section (Fig. 7) showed a vertical columnar structure of the gale zones. Such compact and dense gales column can also result in the lateral oscillation of specific humidity, indicating that the gales could lead to non-uniform horizontal and vertical distributions of water vapor. The large and non-uniform horizontal distribution of wind speed can cause changes in the wind speed gradient along with changes in horizontal divergence. As shown by a strong convergence region (over $-2 \times 10^{-5}$ $s^{-1}$, solid lines) in Fig. 8a, convergence centers correspond to gale centers, which generate severe weather.

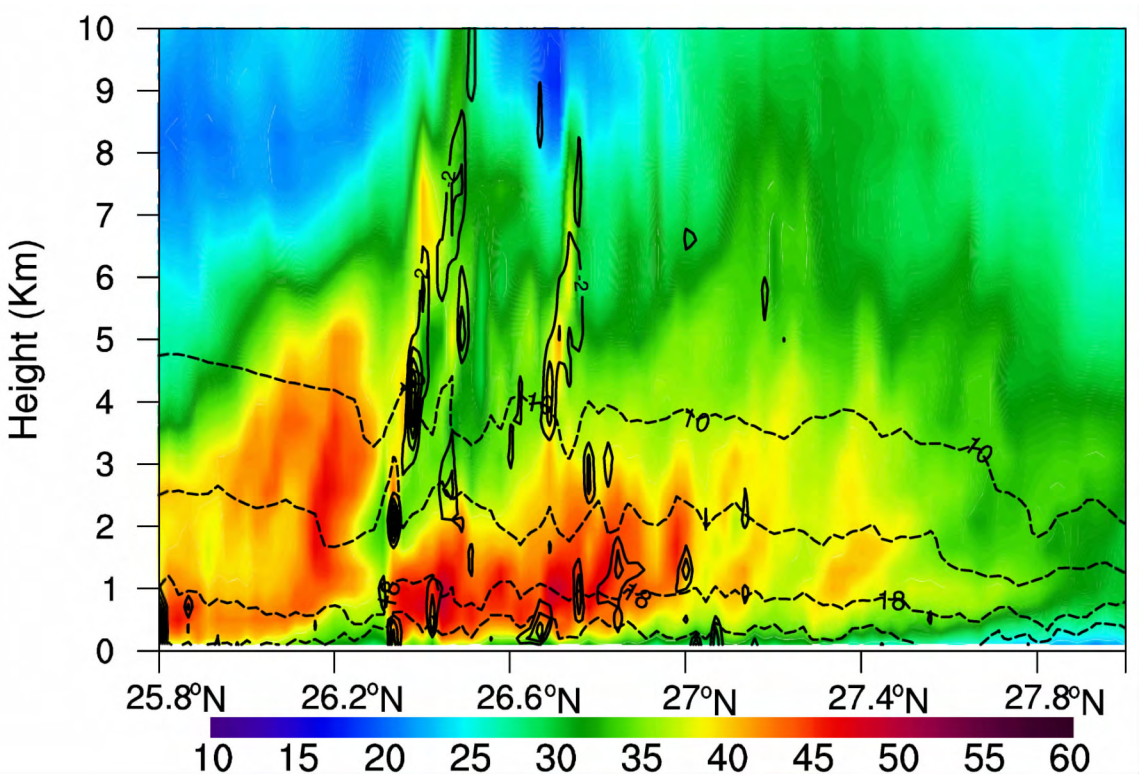


**Figure 7**. Cross-section of simulated winds in domain d03 along M-N in Fig.3c. Wind speed is shown in color, the solid line denotes the convergence line of $\leqslant -2 \times 10^{-5}$ $s^{-1}$, and the dashed line denotes specific humidity. The abscissa shows latitude (°N). The ordinate shows wind speed (m $s^{-1}$).

To focus on the middle and lower troposphere, we plotted the cross-section of wind speed below 2 km along A-B (Fig. 4b). Fig. 8 shows the oscillating and non-uniform offshore gale distribution. The wind speed at the gale center was over 40 m $s^{-1}$, and the MWS was over 55 m $s^{-1}$ near 26.76° E. The gale is shown below 2 km (Fig. 8b). The gale wind speed was reduced to 25 m $s^{-1}$ near the ocean surface, and wave-like, small-scale wind bands were formed, similar to the rolling vortex that occurred over the difference on horizontal wind speed reported by Zhu et al.[17]. The ocean surface wind speed may be significantly reduced to form a vertical column of low wind speed (e.g., near 26.73°E), which could lead to a strong horizontal wind speed gradient along with an imbalance between wind and pressure, resulting in local divergence. This appeared on the two sides of super gale zones and the two sides of low wind speed columns, which caused strong convergence (over $-2 \times 10^{-5}$ $s^{-1}$, Fig.

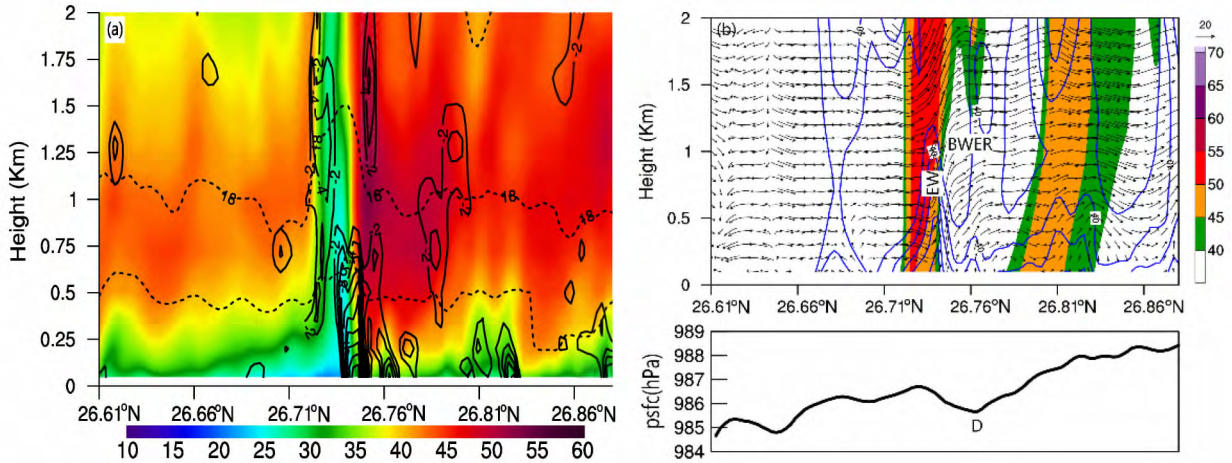


**Figure 8**. (a) Same as Fig. 7 except for simulated winds in domain d05 along A-B in Fig. 4b. (b) Cross section of simulated radar reflectivity (dBz), ageostrophic wind (m $s^{-1}$), and radial vertical circulations of ageostrophic wind (upper panel) and time series of pressure (hPa) and "D" in Fig. 8b for lower pressure (lower panel).

8a). This led to vertical circulation or an increase in vertical circulation, favoring the development of convection (Fig. 8b). The simulated "bounded weak echo region" (BWER) appeared over the gale zone. Because the cross-section is vertical to the wind direction, Fig. 8b mainly displays the vertical flows. On the two sides of the gale, convective echo shows strong convective signals, indicating that the gale caused convective development and strengthened upward motion.

Figure 8a shows that strong convergence appeared below the vertical columns of low wind speed and extended to downstream of the gale. Fig. 8b shows an increase in pressure, and a pressure trough (D) was observed downstream of the gale. The convergence was associated with the low pressure region. The development of the low favored increased convergence and upward motion, leading to the formation of the BWER structure, which is a signal of a severe storm. A geostrophic deviation analysis is made (Kitabatake et al.[30]), see the equation ($V' = V - V_g$, $V_g = -g/f \ \partial Z/\partial n$, where V' is known as the geostrophic deviation or ageostrophic wind, $V_g$ is the geostrophic wind, and V is the simulated wind). The ageostrophic wind is related to the acceleration wind vector, and a typhoon circulation is able to generate strong ageostrophic wind[30]. In terms of the dynamic mechanism, there was a good time corresponding relations in sea level pressure (SLP), divergence and geostrophic deviation of the pressure tough "D". The ageostrophic wind speed increased significantly 10 min before the SLP decreased. During this time, the ageostrophic wind speed increased, and the dynamic convergence caused by the ageostrophic wind reached its greatest intensity (not shown). The ageostrophic wind (blue solid lines in Fig. 8b) and the geostrophic circulation (vectors in Fig. 8b) are very uneven near the convective cloud column. Areas of weak cloud or heave rain are often accompanied by a downward movement of the ageostrophic wind. Meanwhile, the strong convective region is always filled with strong ageostrophic wind and updraft, particularly in the BWER and echo wall (EW). The ageostrophic wind causes strong updrafts and helps form the BWER corresponding to pressure tough "D" ( 26.76 °N ). This phenomenon indicates that the convergence caused by the ageostrophic wind benefits the development of the vertical updrafts over the pressure tough "D". It results in severe weather over the sea, and helps to form the BWER ahead of the convective cloud. The strong gale caused differences in horizontal wind speed and broke the local geostrophic balance, producing ageostrophic wind and resulting in strong convergence on the two sides of gale. Convective clouds correspond to relatively high specific humidity conditions. Warming in clouds and convergence beneath clouds led to the formation of small-scale local low pressure region over the ocean surface, intensifying the cyclonic circulation and gales. This further enhanced mass convergence and upward motion. A trough can be seen in the downstream of gale and convergence region (Fig. 8).

The development of advanced observational technology and increasing computational power have allowed researchers to study mesoscale phenomenon with high resolution simulation. In this study, this high-resolution simulation accurately reproduced the typhoon storm. However, there are many physical portions in numerical model and any change would affect the simulation result. Thus, the characteristics of the structure of this mesoscale wind block's structure in this paper may have some uncertainties caused by geographical conditions, model configuration and temporal and spatial variation.

## 6 CONCLUSIONS

The WRF model was used to simulate offshore gales over Zhejiang and Fujian Provinces associated with Typhoon Soudelor. The results of the simulation using the 333-m grid can be summarized as follows.

(1) The offshore gale distribution produced by the simulation was similar to that indicated by the observational data. The horizontal scale of the gales was 10 –30 km, indicating small-scale gales. The temporal scale of the gales varied. Gales from the ocean were able to reach the bay area, whereas they rapidly weakened over land because of the topography.

(2) Significant pulses in the wind speed occurred during the change in ocean surface gale. The pulses were random and had magnitudes of approximately 5 m $s^{-1}$. The pulses over different locations did not appear in phase, indicating that the possibility of the existence of nonhomogeneous gales and mesoscale strong wind block structures.

(3) The gales near Ningde, Fujian mainly occurred in planetary boundary layers. The gales showed vertical columns, resulting in a horizontal wind speed gradient and thus the oscillation of specific humidity. The gales broke the geostrophic balance and produced ageostrophic wind, resulting in convergence. The strong convergence caused a drop in ocean pressure and thus mass convergence, favoring upward motion and the formation of a BWER structure. Convective clouds were associated with relatively high specific humidity. The warming inside clouds and convergence beneath clouds decreased the local ocean pressure, resulting in locally small-scale low center in ocean area. These physical processes may be responsible for the development of convective clouds and the maintenance of ocean surface gales.

***Acknowledgements:*** The authors would like to thank the Training Center of Atmospheric Sciences of Zhejiang University for their support. The authors would also like to thank Enago (www.enago.cn) for reviewing the English language quality of this paper.

## REFERENCES:

[1] XIN Bao-heng. A Survey of Gale over Yellow Sea and Bohai [M]. Beijing: Meteorological Press, 1991, 191 pp (in Chinese).

[2] YAN Jun-yue, CHEN Qian-jin, ZHANG Xiu-zhi. Climatology over China Offshore [M]. Beijing: Scientific Press, 1993 (in Chinese).

[3] STRETEN N A. Some characteristics of strong wind periods in coastal East Antarctics [J]. J Appl Meteor, 1967, 7(1): 46-52.

[4] STRETEN N A. A review of the climate of Mawson-A representative strong wind site in East Antrarctica [J]. Antarct Sci, 1990, 2(1): 79-89.

[5] LOEWE F. Considerations concerning the winds of Adelie Land [J], Z Gletscherkd Glazialgeol, 1974, 10: 189-197.

[6] REID H J. Modeling coastally trapped wind surges over southeastern Australia. Part I: Timing and speed of propagation [J]. Wea Forecasting, 2000, 14(1): 53-66.

[7] MASS C F, WARNER M D, STEED R. Strong westerly wind events in the Strait of Juan de Fuca [J]. Wea Forecasting, 2014, 29(2): 445-465.

[8] MIGLIETTA M M, ZECCHETTO S, DE BIASIO F. A comparison of WRF model simulations with SAR wind data in two case studies of orographic lee waves over the Eastern Mediterranean Sea [J]. Atmos Res, 2013, 120-121, 127-146.

[9] SHENG Chun-yan, LI Jian-hua, FAN Su-dan. Numerical study of terrain and underlying surface effect on Bohai gale[J]. eteor Mon, 2014, 40(11): 1338-1344 (in Chinese).

[10] CHEN Lian-shou, DING Yi-hui A Survey of Typhoons over Northwestern Pacific [M]. Beijing: Scientific Press, 1979 (in Chinese).

[11] YANG Yu-hua, LEI Xiao-tu. Statistics of strong wind distribution caused by landfall typhoon in China [J]. J Trop Meteor, 2004, 20(6): 633-643 (in Chinese).

[12] LEE W C, MARKS F D. Tropical cyclone kinematic structure retrieved from single Doppler radar observations. Part II: The GBVTD-simplex center finding algorithm [J]. Mon Wea Rev, 2000, 128(6): 1925-1936.

[13] CHEN, Lian-shou, LUO Zhe-xian, LI Ying. Research advances on tropical cyclone landfall process [J]. Acta Meteor Sinica, 2004, 62(5): 541-549 (in Chinese).

[14] LIU Y, ZHANG D L, YAN M K. A multiscale numerical study of hurricane Andrew (1992). Part I: Explicit simulation and verification [J]. Mon Wea Rev, 1999, 125 (12): 3073-3093.

[15] ZHAO K, LEE W C, JOU B J D. Single Doppler radar observation of the concentric eye wall in Typhoon Saomai (2006) near landfall [J]. Geophys Res Lett, 2008, 35(7): 7807-7808.

[16] WANG Zhi-chun, ZHI Shi-qun, DING Lin. Observation and analysis on qiongzhou gales of severe Typhoon Neasat (2011) [J]. J Appl Meteor Sci, 2013, 24 (5): 595-605 (in Chinese).

[17] ZHU P, WANG Y, CHEN S S, et al. Impact of storm-induced cooling of sea surface temperature on large turbulent eddies and vertical turbulent transport in the atmospheric boundary layer of Hurricane Isaac [J]. J. Geophys Res Oceans, 2016, 121(1): 861-876.

[18] MORRISON I, BUSINGER S, MARKS F, et al. An observational case for the prevalence of roll vortices in the hurricane boundary layer [J]. J Atmos Sci, 2005, 62 (8), 2662-2673.

[19] JI Xiao-yang, WU Hui-ding, YANG Xue-lian. A history and current situation on numerical prediction of sea surface wind field [J]. Marine Forecasts, 2005, 22(S1): 167-171 (in Chinese).

[20] GILLIAM R C, PLEIM J E. Performance assessment of new land surface and planetary boundary layer physics in the WRF-ARW [J]. J Appl Meteor Clim, 2010, 49 (4): 760-774.

[21] MIGLIETTA M M, ZECCHETTO S, DE BIASIO F. WRF model and ASAR-retrieved 10m wind field comparison in a case study over Eastern Mediterranean Sea [J]. Adv Sci Res, 2010, 4(1): 83-88.

[22] CHEN Jun-wen, CAI Yang, BAI Yi-ping, et al. Simulation of one gale case in winter in the South China Sea[J]. Marine Forecasts, 014, 31(4): 32-40 (in Chinese).

[23] LIN Y, FARLEY R D, ORVILLE H D. Bulk parameterization of the snow field in a cloud model [J]. J Appl Meteor Clim, 1983, 22(6): 1065-1092.

[24] DUDHIA J. Numerical study of convection observed during the winter monsoon experiment using a mesoscale two-dimensional model [J]. J Atmos Sci, 1989, 46 (20): 3077-3107.

[25] MLAWER E J, TAUBMAN S J, BROWN P D, et al. Radiative transfer for inhomogeneous atmospheres: RRTM, a validated correlated-k model for the longwave[J] J Geophys Res, 1997, 102, 16663-16682.
[26] DUDHIA J. A multi-layer soil temperature model for MM5, PSU/NCAR Mesoscale Model Users Workshop [C]. 1996, 22-24.
[27] KAIN J S. The Kain–Fritsch convective parameterization: an update [J]. J Appl Meteor, 2004, 43(1): 170-181.
[28] CARVALHO D, ROCHA A, GOMEZ_GESTEIRA M, et al. A sensitivity study of the WRF model in wind simulation for an area of high wind energy [J]. Environ Modelling & Software, 2012, 33: 23-34.
[29] ZHANG Zeng-hai, CAO Yue-nan, LIU Tao, et al. Preliminary validation and application of ASCAT scatterometer retrived winds over China offshore seas [J]. Meteor Mon, 2014, 40(4): 473-481 (in Chinese).
[30] KITABATAKE N. Extratropical transformation of Typhoon Vicki (9807): Structural change and the role of upper-tropospheric disturbances [J]. J Meteor Soc Japan, Ser II, 2002, 80(2): 229-247.

**Citation:** ZHU Ye, ZHANG Hong-lei, CHEN You-li, et al. A modeling study of inhomogeneous coastal gales associated with the landfall of typhoon Soudelor (2015) [J]. J Trop Meteor, 2019, 25(1): 1-10.